Publication P3

17.9 A 62µA Interface ASIC for a Capacitive 3-Axis Micro-Accelerometer

Matti Paavola[1], Mika Kämäräinen[1], Jere Järvinen[1], Mikko Saukoski[1], Mika Laiho[1,2], Kari Halonen[1]

[1]Helsinki University of Technology, Espoo, Finland
[2]University of Turku, Turku, Finland

Capacitive accelerometers [1] have advantages such as zero static bias current, the capability of high sensitivity, and excellent thermal stability, making their use in low-power applications attractive. In this paper, an interface ASIC designed for a capacitive 3-axis micro-accelerometer [2] is presented. The die area and power dissipation are reduced by using time-multiplexed sampling and duty cycles down to 0.3%.

The block diagram of the interface with the sensor element [2] is shown in Fig. 17.9.1. The element is composed of four proof masses. The front-end converts the capacitive acceleration information to a voltage. Two algorithmic ADCs convert the acceleration and temperature information into the digital domain. These ADCs are powered down between their conversion cycles. The clock generator provides a 2MHz system clock (SYSCLK), and a 1 to 50MHz microcontroller unit clock (MCUCLK). The latter makes possible more computationally intensive DSP if required. The bandgap-based voltage, current, and temperature reference (V/I/TREF) provides all reference voltages and currents and also temperature information. To provide a more accurate and stable reference current, one off-chip resistor is needed. The operation is controlled by an off-chip DSP.

To reduce the distorting effects of the electrostatic forces, a single-ended self-balancing bridge [3] was chosen as the starting point in the design of the front-end. The power dissipation and die area of the front-end (Fig. 17.9.2) are reduced by using time-multiplexing, thus making possible the reading of one, two, or four proof masses of the 3-axis accelerometer. The clock frequency and biasing currents of the front-end are programmable. Chopper stabilization (CS) and CDS are implemented in order to reduce the offset voltage and noise of the front-end. The front-end controls the voltage of the middle electrode DMID; that is, when measuring at DC, the electrostatic forces are equal in the sensor capacitors CDP(n) and CDN(n), n being the index of the proof mass. The front-end can be used in both differential and single-ended modes. In differential mode, to convert single-ended signals from the sensor element into differential form, the first amplifier is a differential difference amplifier (DDA), making possible the more effective use of signal range in the ADC. The single-ended mode can be used to reduce power dissipation at the cost of reduced dynamic range.

To minimize both power dissipation and silicon area, an algorithmic capacitance ratio-independent ADC was chosen. The ADC architecture is insensitive to capacitance ratio, amplifier offset voltage, and flicker noise. It requires only one differential amplifier, a dynamic latch, 6 capacitors, 36 switches, and some digital logic. Thus, the active die area for a single ADC is only 0.04mm². The structure also makes it possible to use asynchronous and time-multiplexed sampling, requiring only simple control logic. Furthermore, the duty-cycle of the ADC and the respective references is programmable so as to allow more flexible control of current consumption. The operating phases of the implemented ADCs are shown in Fig. 17.9.3. One bit polarity is resolved in four clock steps. The MSB is resolved in phases 1 to 4, and the rest of the bits are resolved by recycling phases 5 to 8. Thus, the total conversion cycle for a 12b operation is 48 clock steps.

The operational amplifiers account for a major part of the current consumption in the front-end and the ADCs. To minimize power dissipation, the tail-current-boosted Class-AB operational amplifier [4] shown in Fig. 17.9.4 is used. The differential input pair M1-M2 is operated in weak inversion in order to maximize the current efficiency g_m/I_D. When the amplifier is used as a comparator in phases 4 and 8 in Fig. 17.9.3, tail-current boosting is disabled by replacing the dynamically controlled current sources M5-M6 with a static current source. When the ADC is powered down, the gates of M3-M8 are pulled to their respective supplies to turn off the transistors, and the common-mode feedback circuit is disabled. In the front-end, the same amplifier topology is used. When operated in differential mode, the DDA is implemented by adding another tail-current-boosted input pair to the normal differential amplifier.

The SYSCLK is based on a source-coupled CMOS multivibrator, whose oscillation frequency is calibrated to 2MHz at room temperature using on-chip resistor and capacitor matrices. The MCUCLK, using a 1.2V supply, is a 3-stage single-ended current-starved ring oscillator with its oscillation frequency tunable from 1 to 50MHz. The V/I/TREF is based on Brokaw's bandgap reference [5]. The reference voltages of 1.2 and 0.9V are generated using two load resistors in series at the output stage of the feedback amplifier. The current reference of 1µA is generated by using the 1.2V reference voltage and a 1.2MΩ off-chip resistor driven by an on-chip voltage buffer. The inherent PTAT voltage of the bandgap reference is exploited by the TREF. The buffered and amplified PTAT voltage is converted by the TREF ADC. Because the temperature changes slowly, a duty-cycle of 0.3% is used to reduce the current consumption of the TREF and the TREF ADC to negligible levels.

The prototype was fabricated in a 0.13µm CMOS technology, using MIM capacitors and high-resistivity resistors. The active area of the chip (Fig. 17.9.7) is 0.51mm². The chip was combined with an external ±4g capacitive 3-axis accelerometer on a PCB. The measured FFT plot for z-directional -1g acceleration is shown in Fig. 17.9.5. The measured noise densities in the x, y, and z directions with a 1kS/s sampling frequency are 460µg/√Hz, 550µg/√Hz, and 550µg/√Hz, respectively. These results yield a dynamic range of 65dB at the 100Hz bandwidth. The results are expected to improve when the interface is bonded directly to the sensor. Figure 17.9.5 also shows measured arbitrary accelerations in all three directions.

The core of this sensor ASIC without the MCUCLK draws 62µA from a 1.8V supply while sampling temperature at 100S/s and four proof masses, each at 1kS/s. The overall performance is summarized in Fig. 17.9.6.

References:
[1] M. Lemkin et al., "A 3-Axis Surface Micromachined ΣΔ Accelerometer," *ISSCC Dig. Tech. Papers*, pp. 202-203, 1997.
[2] T. Lehtonen and J. Thurau, "Monolithic Accelerometer for 3D Measurements," *Advanced Microsystems for Automotive Applications*, pp. 11-22, J. Valldorf, W. Gessner Eds., Springer, 2004.
[3] H. Leuthold and F. Rudolf, "An ASIC for High-Resolution Capacitive Microaccelerometers," *Sens. Actuators A*, vol. 21, pp. 278–281, Feb., 1990.
[4] R. Harjani, R. Heineke and F. Wang, "An Integrated Low-Voltage Class AB CMOS OTA," *IEEE J. Solid-State Circuits*, pp. 134–142, Feb., 1999.
[5] A. P. Brokaw, "A Simple Three-Terminal IC Bandgap Reference," *IEEE J. Solid-State Circuits*, pp. 388–393, Dec., 1974.
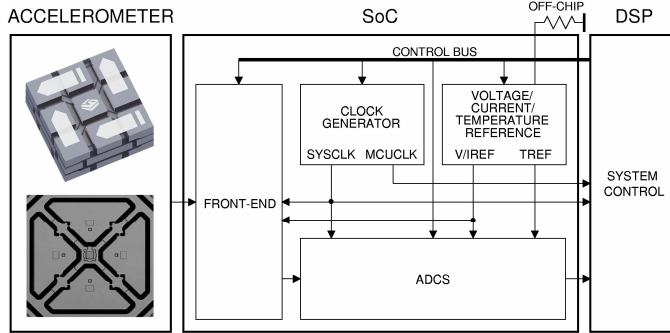
Figure 17.9.1: Block diagram of the interface for a 3-axis capacitive micro-accelerometer. The encapsulated accelerometer [2] is shown at top left. A top view of the structural wafer of the accelerometer is shown bottom left. (Images courtesy of VTI Technologies, Vantaa, Finland.)
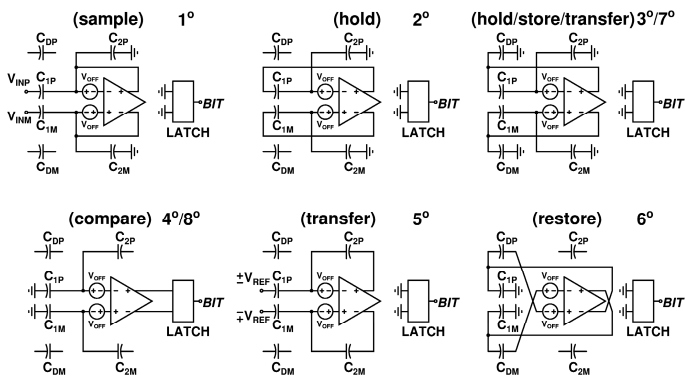
Figure 17.9.2: Schematic of the front-end.

Figure 17.9.3: Operating phases of the ADCs.

Figure 17.9.4: Operational amplifier used in the ADCs. Top: core amplifier, Bottom: double-sampling common-mode feedback circuit.
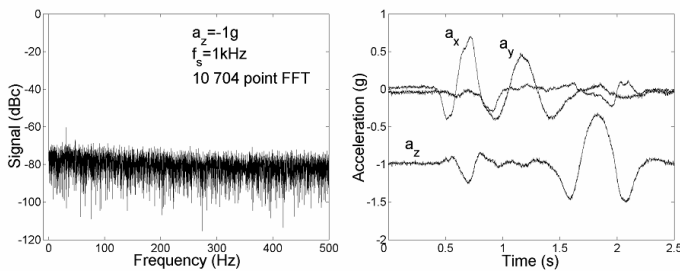
Figure 17.9.5: Left: the measured FFT plot for z-directional -1g DC acceleration, Right: measured arbitrary accelerations in all three directions.
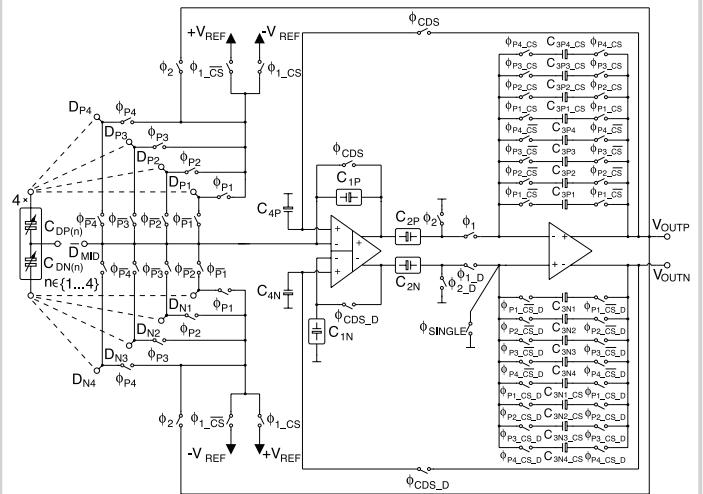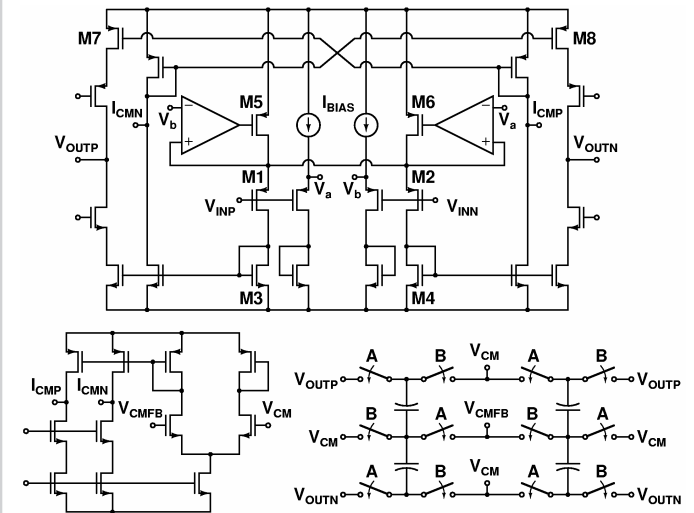
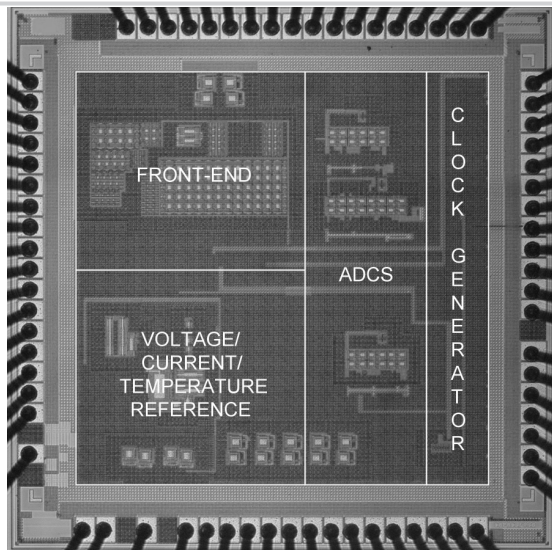| Process	0.13μm CMOS with MIM capacitors and high-resistivity resistors						
V_{DD}	1.8V						
Mode	Single-ended			Differential			
f_S / mass	100	1 000	10 000	100	1 000	10 000	(Hz)
I_{AVG}	47	54	216	54	62	217	(μA)
Noise floor							
x-axis	2 130	680	240	1 770	460	280	(μg/√Hz)
y-axis	2 650	840	280	1 920	550	390	(μg/√Hz)
z-axis	2 650	840	280	1 920	550	390	(μg/√Hz)
TREF	0.18						(K)
Active area	0.51						(mm²)

Figure 17.9.6: Performance summary.

17

Figure 17.9.7: Chip micrograph.